

# Spectroscopic Observations of Optically Selected Clusters of Galaxies from the Palomar Distant Cluster Survey<sup>1</sup>

B. P. Holden<sup>2</sup>

Department of Astronomy and Astrophysics, University of Chicago, 5640 South Ellis Ave.  
Chicago, Illinois 60637  
holden@oddjob.uchicago.edu

R. C. Nichol, A. K. Romer<sup>2</sup>

Department of Physics, Carnegie Mellon University, 5000 Forbes Ave. Pittsburgh,  
Pennsylvania 15213-3890  
nichol@andrew.cmu.edu, romer@andrew.cmu.edu

A. Metevier<sup>2</sup>

Department of Astronomy and Astrophysics, University of California, Santa Cruz,  
California 95064  
anne@ucolick.org

M. Postman<sup>2</sup>

Space Telescope Science Institute<sup>3</sup>, 3700 San Martin Dr., Baltimore, Maryland 21218  
postman@stsci.edu

M. P. Ulmer

Department of Physics and Astronomy, Northwestern University, 2131 Sheridan Road,  
Evanston, Illinois 60208-2900  
m-ulmer2@nwu.edu

L. M. Lubin

California Institute of Technology, 105-24 Caltech, 1201 East California Blvd, Pasadena,  
California 91125  
lml@astro.caltech.edu

---

<sup>1</sup>Based on observations obtained with the Apache Point Observatory 3.5-meter telescope, which is owned and operated by the Astrophysical Research Consortium.

<sup>2</sup>Visiting Astronomer, Kitt Peak Observatory, National Optical Astronomy Observatories, which is operated by the Association of Universities for Research in Astronomy (AURA), Inc., under cooperative agreement with the National Science Foundation.

<sup>3</sup>The Space Telescope Science Institute is operated by the AURA, Inc., under National Aeronautics and Space Administration (NASA) Contract NAS 5-26555.

## ABSTRACT

We have conducted a redshift survey of sixteen cluster candidates from the Palomar Distant Cluster Survey (PDCS) to determine both the density of PDCS clusters and the accuracy of the estimated redshifts presented in the PDCS catalog (Postman *et al.* 1996). We find that the matched-filter redshift estimate presented in the PDCS has an error  $\sigma_z = 0.06$  in the redshift range  $0.1 \leq z \leq 0.35$  based on eight cluster candidates with three or more concordant galaxy redshifts.

We measure the low redshift ( $0.1 \leq z \leq 0.35$ ) space density of PDCS clusters to be  $31.3_{-17.1}^{+30.5} \times 10^{-6} h^3 \text{Mpc}^{-3}$  (68% confidence limits for a Poisson distribution) for Richness Class 1 systems. We find a tentative space density of  $10.4_{-8.4}^{+23.4} \times 10^{-6} h^3 \text{Mpc}^{-3}$  for Richness Class 2 clusters. These densities compare favorably with those found for the whole of the PDCS and support the finding that the space density of clusters in the PDCS is a factor of  $\simeq 5$  above that of clusters in the Abell catalog (Abell 1958; Abell *et al.* 1989). These new space density measurements were derived as independently as possible from the original PDCS analysis and therefore, demonstrate the robustness of the original work. Based on our survey, we conclude that the PDCS matched-filter algorithm is successful in detecting real clusters and in estimating their true redshifts in the redshift range we surveyed.

Keywords: galaxies: clusters: general — catalogs

## 1. Introduction

One of the focal points of modern observational cosmology is the determination of the matter density of the universe. Measurements of the abundance of clusters of galaxies provide some of the strongest constraints on this cosmological parameter. For example, in a high density ( $\Omega_m = 1$ ) universe, one would predict rapid evolution in the number density of massive clusters with redshift, while in a low density ( $\Omega_m \ll 1$ ) universe, one would expect an almost constant number density of such systems (Lacey & Cole 1993; Viana & Liddle 1996; Oukbir & Blanchard 1997; Bahcall *et al.* 1997; Reichart *et al.* 1999).

In the past, it has been difficult to measure the number density of massive clusters from optically-selected samples of clusters because previous samples have typically lacked a quantifiable selection function (*e.g.* Gunn *et al.* 1986; Abell *et al.* 1989; Couch *et al.* 1991). However, in recent years, the emergence of optical cluster catalogs created with a

completely automated selection (Lumsden *et al.* 1992; Dalton *et al.* 1992; Postman *et al.* 1996 or P96; Lidman & Peterson 1996) have now made it possible to use optically selected catalogs for space density measurements. For example, the Palomar Distant Cluster Survey (PDCS; which is contained in P96) was the first fully-automated, objectively-selected cluster catalog to be based on deep CCD imaging data. The cluster catalog was constructed from a galaxy survey covering  $5 \text{ deg}^2$  to  $V = 23.8$  ( $3\sigma$  completeness). The PDCS contains 79 cluster candidates selected via a matched-filter algorithm that used both the magnitude and positional data of the galaxies to find clusters. This matched-filter is based on a model for the galaxy distribution; a King profile for the positional data and a Schechter function for the luminosity distribution of the galaxies in the clusters. The strength of any observed correlation of the data with this matched-filter can be used to measure how well the model matches the data, with the strongest correlations being assigned to cluster candidates. In this way, the PDCS also generated an estimated redshift, a galaxy richness and other parameters for each cluster candidate based on the best-fitting model.

Using the original catalog of 79 clusters, P96 discovered two important results. First, they determined that the space density of PDCS clusters, for a given Richness class, was constant with redshift. Second, they showed that the measured space density of PDCS clusters was a factor of  $\sim 5 \pm 2$  above that seen in the local universe as measured from the Abell catalog (see P96 for a discussion of the Abell catalog space density). These results have important implications and have already been used to constrain cosmological parameters. For example, Bahcall *et al.* (1997) used the observed constant space density of PDCS clusters with redshift, along with other samples of clusters, to constrain both  $\Omega_m$  and  $\sigma_8$  (the variance of density perturbations on cluster scales). Bahcall *et al.* (1997) found that the PDCS space density was consistent with a low  $\Omega_m$  cosmological model. These results illustrate the potential of objectively-selected, statistical catalogs of clusters to constrain cosmological models. The work of Bahcall *et al.* (1997), however, rests on several untested assumptions about the intrinsic properties of the PDCS clusters i.e. their M/L ratio, estimated redshifts *e.t.c.*, some of which will be discussed in this paper.

Computer-based optical cluster finding algorithms such as the matched-filter used to produce the PDCS will certainly play a major role in the construction of the next generation of catalogs of clusters of galaxies. This has already started to happen with surveys such as DeepRange (Postman *et al.* 1998), the ESO Imaging Survey (Olsen *et al.* 1999a; Olsen *et al.* 1999b), the MDS deep cluster sample (Ostrander *et al.* 1998) and the survey of Zaritsky *et al.* (1997) to name but a few. As the size and redshift range of the catalogs increase, more detailed studies of the cluster evolution will be possible providing tighter constraints on the values of  $\Omega_m$  and  $\sigma_8$ . Therefore, our group has embarked on a long-term program to study the properties of the clusters discovered by the matched-filter algorithm.

In this paper, we present the results of a redshift survey of a subset of PDCS cluster candidates designed to test the estimated redshifts of these cluster candidates as well as re-measuring the space density of the PDCS catalog using spectroscopic redshifts. We designed this redshift survey to select a statistical subsample of PDCS cluster catalog which is independent of most of the cluster parameters derived by P96. This approach minimizes the effect on our conclusions of any systematic errors in those parameters. In Sec. 2 of this paper, we discuss how we selected the cluster candidates for this present spectroscopic survey. Sec. 3 describes the spectroscopic observations and data reduction. We then characterize the distribution in redshift of the clusters in Sec. 4. In Sec. 5, we discuss the implications of our results and we conclude in Sec.6 with a summary of this paper.

## 2. PDCS Cluster Candidate Selection

Thirteen of the sixteen target clusters used in our spectroscopic survey were selected from the subsample of PDCS clusters randomly observed by the ROSAT satellite (as discussed in Holden *et al.* 1997). These X-ray observations detected emission near six PDCS cluster candidates and measured upper-limits for twenty-five PDCS cluster candidates. Three of the six PDCS cluster candidates found associated with X-ray emission in Holden *et al.* (1997) are part of the sample discussed in this paper. The remaining three (PDCS 11, 12 & 23) were taken from the rest of the PDCS.

The main goals of our spectroscopic survey were to check the measured space density of PDCS clusters and the accuracy of the estimated redshifts. Therefore, we selected our targets as independently as possible of the derived parameters given by P96. We selected targets using only the net number of  $V_4 < 21$ ,  $V_4 - I_4 > 1$  galaxies (the subscript 4 refers to the 4-Shooter camera used to construct the PDCS, see P96 for details on the filter system used and the resulting galaxy catalog) within a 2'.5 radius aperture of the PDCS cluster candidates' position. By taking this approach, we still select clusters that potentially have a true redshift vastly different from the PDCS estimated redshift. Such clusters would have been ignored if we had imposed a matched-filter estimated redshift cut-off.

We chose the above magnitude limit, color limit and angular size to maximize the number of cluster candidates we could observe given the limitations of our instrumentation. The color criterion was chosen to maximize the number of prospective cluster members over field galaxies. The median color of the field galaxies in the PDCS is  $V_4 - I_4 \simeq 1$ , while the cluster members are usually redder than this limit (Lubin 1996). We note here that this color selection does bias us against clusters dominated by blue galaxy members. The aperture size we chose was simply the field of view of the Cryogenic Camera spectrograph,

one of the two instruments we used.

To compute the number of galaxies in our aperture, we filtered the PDCS galaxy catalog removing all galaxies fainter than our magnitude limit and bluer than our color limit. We then counted the number of galaxies within the 2'.5 radius aperture centered on each PDCS cluster candidate's position. We subtracted the expected number of field galaxies from the number of galaxies in the aperture to obtain an estimate of the net number of cluster candidate galaxies per aperture. The expected number of galaxies was computed for each of the four different PDCS fields (00<sup>h</sup>, 02<sup>h</sup>, 09<sup>h</sup> and 13<sup>h</sup>) separately. The surface density of field galaxies was measured by finding the total number of galaxies in our filtered catalog not within the 2'.5 radius of a PDCS cluster candidate and then dividing that number by the area covered by the catalog but excluding the area within 2'.5 of PDCS cluster candidates.

We ranked the 31 PDCS cluster candidates from the analysis of Holden *et al.* (1997) based on the net number of cluster galaxies as calculated above. We then observed the PDCS cluster candidates in descending order on this list. In this way, we ensured that any partial subset of this sample of 31 would be complete. We eventually observed the top thirteen of these 31 candidates and these thirteen clusters are listed in Table 1. We observed three other clusters (PDCS 11, 12 & 23) that are not part of this complete sample but were nonetheless selected in the same way (and are also listed in Table 1.) In Figure 1, we plot the clusters we observed (with stars) and the clusters we did not observe (with circles) as a function of their PDCS estimated redshift and estimated richness. Immediately one can see that most of the clusters we observed possess a low estimated redshift and a high estimated richness. Also apparent are two clusters (PDCS 41 and 42) that have a high estimated redshift and a low estimated richness. These clusters will be discussed in Sec 4.3.

### 3. Spectroscopic Data and Reduction

We spectroscopically observed a total of 130 galaxies in the direction of the sixteen PDCS cluster candidates discussed above (Table 1). These observations were carried out on either the Kitt Peak National Observatory (KPNO) Mayall 4 meter or the ARC 3.5 meter telescope at Apache Point Observatory (APO). Below we discuss the process of creating slit masks for the KPNO observations and galaxy selection for the observations performed on both telescopes.

### 3.1. KPNO Masks and Observations

We observed 122 galaxies towards fifteen of the sixteen PDCS cluster candidates in our survey on the KPNO Mayall 4 meter using the Cryogenic Camera with the 770 Grism (blazed with a peak transmission at  $\sim 6000\text{\AA}$ ) or the 780-2 Grism (blazed with a peak transmission at  $\sim 7100\text{\AA}$ ) using multi-object slit masks. The observations were carried out over six nights from April 29, 1997 to May 1, 1997 (KPNO1 on Table 1) as well as December 19, 1998 and December 21, 1998 (KPNO2 on Table 1). All of the multi-slit masks were constructed using a constant slit width of  $2''.5$  and a slit length of at least  $14''$ .

For every cluster candidate, our aim was to observe a statistical subsample of the galaxies that met our original color ( $V_4 - I_4 > 1$ ) and magnitude criteria ( $V_4 < 21$ ). Therefore, to construct a mask, we weighted each galaxy linearly based on its observed color with the highest priority going to the reddest galaxies. This was done to maximize the number of galaxies with strong absorption features typical of the old, metal-rich, ellipticals typically found in the cores of clusters. The magnitude of the galaxies played no part in the determination of the weights as we did not want to bias ourselves against fainter, and possibly higher redshift, galaxies that met our magnitude limit. To obtain the optimal use of the multi-slit masks, we also included galaxies blue-ward of our color cut but these galaxies were only used when a “red” ( $V_4 - I_4 > 1$ ) galaxy could not be targeted. To achieve this, the “blue” galaxies were given uniform weights one hundred times smaller than the smallest possible weights given to the “red” galaxies. One multi-slit mask was constructed for each cluster candidate with the final galaxy selection being performed automatically by maximizing the total weight for each mask. In addition to galaxies, each mask required an alignment star ( $15 < V < 17$ ) which was critical for ensuring that our target galaxies were aligned within the slit-lets. In some cases, we were forced to move the desired mask centers away from the original PDCS cluster centroid to obtain alignment stars. The worst case was PDCS 60 which had to be shifted by  $1'$  leaving only four slit-lets within the  $2.5'$  aperture used for candidate selection. The details of the observing are summarized in Table 1, including the position of the center of the masks and the number of slit-lets per mask.

During our six nights at KPNO we encountered variable seeing and transparency which resulted in only 77 useful spectra out of the 122 galaxies observed. For each mask, we also obtained He, Ne, and Ar arc lamp calibration spectra as well as quartz spectral flats at the same zenith angle. For a few of the longer integration times, we obtained arc calibrations before and after the observation, though we did not see any noticeable difference in the arc line positions.

All the multi-slit spectral data were reduced as outlined in Ellingson (1989) using the IRAF aperture spectra package, APEXTRACT. The spectral flat field observations

were used to remove the CCD response function. We found tracing the spectrum using a third order Legendre polynomial yielded the best results and we found the background to be well fit by a constant. We used variance-weighted extraction to produce the one dimensional spectra. These one-dimensional spectra were wavelength calibrated with the arc calibrations. The resulting spectral coverage was 4000Å to 9000Å in pixels of 4.75Å for the 770 Grism. We measured a resulting resolution of 14.9Å using the width of the arc calibration lines for the same Grism. For the 780-2 Grism, the spectra covered 4500Å to 9500Å with at 4.5Å per pixel with a resolution of 14.4Å. In Figure 2, we present some examples of our spectra.

### 3.2. ARC Data

We observed eight galaxies for PDCS 02 and 05 on the ARC 3.5m at APO with the Double Imaging Spectrograph (DIS) on October 4th and October 26th, 1997. All observations were carried out with a long slit rotated to observe two galaxies at once. The DIS instrument possesses a dichroic which splits the incoming beam into a blue camera, covering a wavelength range of 3800Å to 6000Å with 6.3Å per pixel, and a red camera, which covers a wavelength range of 5000Å to 9000Å with 7Å per pixel. The resolution of the red camera is measured to be 24.5Å while the resolution of the blue camera is 10.6Å based on the full-width at half-maximum of arc calibration lines.

At the time of the observations both DIS cameras had high read noise, the blue CCD chip had a read noise of 15 e<sup>-</sup> while the red CCD chip had 28 e<sup>-</sup>. The blue chip is comparable with the Cryogenic Camera CCD chip in terms of read-noise and quantum efficiency so we relied on data mostly from this camera for making the redshift identifications of our target objects. We used the data from the red camera only to search for emission lines.

Our galaxy selection was done in a similar manner as discussed above for the Cryogenic Camera. As we were not using multi-slit masks, we did not need to include any of the “blue” objects discussed above, we simply sorted the “red” target galaxies ( $V_4 - I_4 \geq 1.0$ ) in our 2.5 radius fields by magnitude and began by observing the brightest objects. PDCS 02 was also observed at KPNO with the CryoCam spectrograph yielding a total of seven useful spectra (three from the KPNO observing run and four from the ARC observing run). Table 2 presents the data from both instruments.

We obtained spectral flats as well as He and Ar arc lamps calibrations at the beginning of every night. We tested the dispersion corrections using sky lines and found them to be

stable at the low resolutions we used. For some objects a small shift on the order of a half a pixel was required. Each spectrum was shifted appropriately before we determined the redshift of the target object.

As with the Cryogenic Camera data, we used variance-weighted extraction to create our one dimensional spectra. We then combined the red and blue spectra using SCOMBINE in IRAF to produce one spectrum for each galaxy from 3800Å to 9000Å with 6.3Å per pixel, Figure 2 shows one such spectrum.

### 3.3. Galaxy Redshift Determination

Overall, we obtained spectra for 130 galaxies but, as mentioned above, not all these spectra yielded a redshift measurement. We present in Table 2 the 84 galaxies for which we obtained a redshift, 77 from KPNO and 7 from the ARC 3.5m. These redshifts were determined either by using the IRAF command RVIDLINES to fit profiles to emission lines or by using the RVSAO package (Kurtz & Mink 1998) to cross-correlate the spectra with absorption line galaxy templates.

Only six of the galaxy spectra have obvious emission lines. This is a likely result of the color selection criterion we imposed on the targeted galaxies. For PDCS 57 #2, we have both an absorption and emission line redshift which agree with each other within the estimated errors.

All 130 galaxies were processed using the XCSAO procedure in the RVSAO package. The XCSAO command cross-correlates the spectrum with a number of template spectra. We used three template spectra provided in the RVSAO package (M31, M32 and a sum of 1489 spectra called fabtemp97, see Kurtz & Mink 1998 for details on this last template). Before cross-correlation, we removed the parts of the spectra around bright sky lines, and the large Telluric absorption features, as many of our spectra possessed large residual errors in these regions due to inaccurate sky subtraction. This can be seen in Figure 2. We also trimmed the wavelength coverage of our spectra before cross-correlating. In general, for the KPNO spectra, we trimmed off the first 500Å and the last 500Å. For some spectra, not all of the wavelength range could fit within the CCD image, so we further trimmed the spectrum before cross-correlating.

In Table 2 we provide the PDCS identification number, the identification number assigned to that galaxy in the mask, the J2000 coordinates of the galaxy, the galaxy’s  $V_4$  magnitude, the  $V_4 - I_4$  color, the redshift with error, and the Tonry & Davis (1979)  $r$  value from the cross-correlation for absorption spectra. We consider all redshifts with  $r > 3$  to be

secure measurements, as recommended by Kurtz & Mink (1998). Emission line spectra are marked with the letter “e” in the last column followed by the number of lines used to fit the redshift. We note here that the spectrum of PDCS 61 # 112 shows evidence for an active galactic nucleus, *i.e.* one very wide emission line (see Figure 2). We assign a tentative redshift to this active galactic nucleus candidate assuming the emission lines is Mg II at 2798Å. PDCS 57 # 110 is listed twice in Table 2, one listing for the emission line redshift and one listing for the absorption line redshift.

## 4. Cluster Redshift Distribution and Space Density

As stated before, the main goal of our spectroscopic survey was to determine the space density of PDCS clusters and to test the estimated redshifts derived from the matched-filter algorithm. Below we discuss how we determined the global redshift of the observed PDCS cluster candidates as well as discussing the probable error on the PDCS estimated redshift. We then discuss our derivation of the space density of PDCS clusters via Monte Carlo simulations of our selection process.

### 4.1. Determining Cluster Redshifts

Given the individual galaxy redshifts, we need to determine which PDCS cluster candidates are likely to be real physical systems and assign to them a global cluster redshift. For our first estimate of the true cluster redshift, we found the median redshift of all the galaxies observed towards that cluster candidate. In Table 3, we list for each of our sixteen PDCS cluster candidates this median redshift. We also list our estimate of the “best” cluster redshift. In cases where we have three or more concordant cluster members within 1500 km s<sup>-1</sup> of the median redshift, the median redshift of all of the cluster galaxies is assigned as the “best” cluster redshift. We chose 1500 km s<sup>-1</sup> as it is approximately three times the typical cluster velocity dispersion as given by Girardi *et al.* (1998). However, for the seven cluster candidates for which we only have two redshift measurements that agree to within 1500 km s<sup>-1</sup>, we simply average these two measurements and quote this as the “best” cluster redshift. PDCS 57 does not have a pair of galaxies within a 1500 km s<sup>-1</sup> velocity separation, therefore we leave the “best” redshift estimate blank. The final column in Table 3 provides the fraction of galaxy redshifts we measured to be within 1500 km s<sup>-1</sup> of the “best” redshift. Also presented in Table 3 is an error estimate on the “best” redshift. This error is only quoted for the eight clusters with three or more galaxies in agreement. The error listed is the median absolute deviation of the galaxy redshifts in km s<sup>-1</sup>. The

value for PDCS 02 is quite high because of the large number of redshifts (four out seven) that are not near the median redshift, thus leading to a possibly large over-estimate of the error for the cluster redshift.

P96 predicts that  $> 10\%$  of all PDCS clusters are likely false detections from Monte Carlo simulations. Therefore, it is possible that one, or two, of our spectroscopically observed PDCS cluster candidates is not a real, physical cluster. This problem becomes more acute when we note that seven of our sixteen observed PDCS cluster candidates only have two galaxies close in redshift space (within  $1500 \text{ km s}^{-1}$  of each other). To measure the frequency of such close pairs of galaxies in the field population of galaxies, we randomly sampled the Canada-France Redshift Survey (CFRS; Lilly *et al.* 1995; LeFevre *et al.* 1995; Hammer *et al.* 1995; Crampton *et al.* 1995). Using the same color and magnitude limits, adjusted for slight differences in the filters used, we extracted random groups of galaxies from the CFRS database, regardless of their angular distribution. Initially, we chose a size of three galaxies as this corresponded to the lowest number of galaxy redshifts we observed towards any one of our sixteen PDCS candidates (see Table 1). From these simulations, we discovered that  $\sim 16\%$  of all groupings of three galaxy redshifts, extracted from the CFRS, possess a pair of galaxy redshifts with a separation less than or equal  $1500 \text{ km s}^{-1}$  or less. If we increase the grouping size to four galaxy redshifts extracted at once from the CFRS, the situation becomes worse, with a close pair (within  $1500 \text{ km s}^{-1}$ ) occurring  $\sim 27\%$  of the time. For a grouping size of five galaxies, we find a close pair of galaxies  $\sim 41\%$  of the time.

If we increase our requirement to observing a triplet of galaxies, all within  $1500 \text{ km s}^{-1}$  of either side of their median redshift, then the above rates of such an occurrence, as observed from the CFRS database, drop dramatically to  $\sim 3\%$  for a grouping size of five galaxy redshifts. Using these numbers as a guide, for the remainder of this paper, we will consider those eight PDCS cluster candidates which possess three or more galaxy redshifts within  $1500 \text{ km s}^{-1}$  of the median redshift as detected clusters.

## 4.2. Matched-Filter Redshifts

We have used our measured cluster redshifts to test the matched-filter redshift estimate given by P96. In Figure 3, we plot the estimated redshift versus our spectroscopically measured redshift as well as the expected  $45^\circ$  line for comparison. In this plot, the solid squares represent cluster candidates with three or more concordant redshifts, while the open circles represent clusters with only two redshifts in agreement.

To quantify the observed accuracy of the matched-filter redshifts, we calculated

the standard deviation of the difference between the matched-filter redshift and the spectroscopically measured redshift. If we include only the eight clusters with three or more concordant galaxy redshifts, as discussed above, the standard deviation is  $\sigma_z = 0.06$ .

In Figure 3 there are two significant outliers; PDCS 41 and 42. For these two PDCS cluster candidates, the galaxies we have spectra for are near the cluster centroid but are significantly brighter in magnitude than we would expect for any cluster members at the estimated redshift of these two cluster candidates (see Figure 9 of P96 which shows that for  $z \simeq 0.8$  clusters, one would not expect to see a single cluster member brighter than  $V_4 = 21.5$ ). For these two cluster candidates therefore, we have either found a low-redshift group masquerading as a high redshift cluster (with a significantly different luminosity function), or we have found a chance superposition of a pair of galaxies at low redshift (see the above discussion concerning the probability of this happening). In either case, we can not rule out the presence of a high redshift cluster near the estimated redshift for PDCS 41 and 42.

For completeness, if we include all fifteen of our PDCS cluster candidates with at least two galaxies within  $1500 \text{ km s}^{-1}$ , the standard deviation between the measured and matched-filter redshift rises to  $\sigma_z = 0.20$ , which is in good agreement with the error quoted by P96. The increase in the error is mainly caused by the two outliers discussed above (PDCS 41 and 42). If we exclude PDCS 41 and 42, the error drops to  $\sigma_z = 0.07$ .

### 4.3. The Space Density of PDCS Clusters

We do not possess a volume limited sample of clusters because of the selection criteria used in the creation of our sample. Therefore, we performed Monte Carlo simulations of our selection procedure to estimate the range in redshift covered by our survey. To compute the probability of a cluster being selected for our survey, we constructed model PDCS clusters and simulated the selection process outlined in Sec 2. We performed these simulations 10000 times to compute the probability that we would detect PDCS clusters at different redshifts. These probabilities were then multiplied by the volume element at that redshift (assuming a  $q_0$  and  $H_0$ ) to produce an effective volume for a cluster with a given set of properties. These simulations can then be used to determine the redshift range over which our survey is mostly complete and hence statistically correct our incompleteness.

In our simulations, the clusters were modeled using a Schechter luminosity function and a King model for the density profile. The parameters controlling the shape of the cluster luminosity function and spatial profile were allowed to vary within their observed

distributions. For the King profile, we used the median core radius ( $r_c = 0.050 \text{ Mpc h}^{-1}$ ) and slope ( $\alpha = -1.36$ ) as estimated by Lubin & Postman (1996) (see Table 2) for the PDCS. We also used the variance estimates quoted by these authors. For the Schechter luminosity function, we assumed  $M_\star = -21.1$  in the  $V_4$  band and a slope of  $\alpha = -1.1$ , which are the values used in P96. For the variance estimates of the luminosity function we used the values quoted in Colless (1989). A random normalization (denoted  $\Lambda$  in P96) drawn from the actual values found in the PDCS was used for each luminosity function. These normalizations, however, were restricted to the ranges of Richness Class 0 ( $20 \leq \Lambda_V \leq 40$ ), 1 ( $40 \leq \Lambda_V \leq 60$ ), and 2 ( $60 \leq \Lambda_V \leq 80$ ) type clusters. We would like to note here that the richness we use,  $\Lambda$ , has a redshift dependence (see Figure 19 of P96). However, in the range of redshifts we are interested in,  $0.1 \leq z \leq 0.5$ , the redshift dependence is quite mild so the above ranges of  $\Lambda_V$  reproduce the corresponding Abell Richness Classes (see Fig. 17 of P96).

For each cluster, we assumed that the luminosity function only contains galaxies redder than our color criterion,  $V_4 - I_4 > 1$ . This assumption is not strictly correct, however, the majority ( $\gtrsim 80\%$ ) of all galaxies in PDCS cluster candidates are redder than our color criterion (see Figure 7 of Lubin 1996).

We note here that the apparent magnitudes of our simulated galaxies depend not only on the cosmology and the luminosity function but also on the k-corrections. We used the k-corrections of an elliptical-type galaxy (the nuclear bulge of M31) from Coleman *et al.* (1980) with linear interpolation between the tabulated values. We chose an elliptical galaxy spectral energy distribution as this is most consistent with the red galaxies found in the cores of these rich clusters. We used two values of the deceleration parameter,  $q_0$ , 0.5 and 0.1. All of our results are computed with a Hubble Constant of  $H_0 = 100 \text{ km s}^{-1} \text{ Mpc}^{-1}$ .

For each simulated cluster, we computed the expected number of cluster galaxies to fall within a  $2.5$  aperture and above a magnitude limit of  $V_4 = 21$ . We computed a Poisson deviate from this expectation value. We then computed another Poisson deviate using the average number of background galaxies meeting our galaxy selection criteria that fall within the  $2.5$  aperture as the expectation value. The sum of these two deviates is the simulated number of galaxies. From this number, we subtract the surface density of field galaxies. This difference is the net number of galaxies in our aperture.

We performed the above simulation 10000 times for a given Richness Class at each redshift interval of 0.01 out to  $z = 0.6$ . At each redshift, we computed the percentage of times the net galaxy count exceeded 2.5 galaxies, (the smallest net galaxy number listed in Table 1). This percentage provided an estimate of the probability of such a cluster being included in our observing sample. These probabilities are summarized in Figure 4 for

Richness Class 0 and 1 clusters as a function of redshift and for  $q_0 = 0.5$  (solid lines) and  $q_0 = 0.1$  (dashed lines).

As can be seen from Figure 4, all model clusters, at any redshift, have a finite probability of being included in our sample. This is the result of chance fluctuations in the background being large enough to cause a cluster to be selected even though none of the cluster members would actually fall within our magnitude limit. This is a plausible explanation for why PDCS 41 and 42 are included in our sample even though they have estimated redshifts so high that none of the cluster members should be brighter than our magnitude limit. If we assume that the field galaxy population follows a Poisson distribution, we can calculate the expected number of times that a fluctuation in the background would result in a high redshift cluster falling in our sample, such as PDCS 41. We calculated this would happen 18% of the time for such clusters. This agrees quite well with the results of our Monte Carlo simulations (see Figure 4) and thus provides a check on our method.

Using the results of the above simulations, we can now compute the probability of a cluster being selected for our survey. However, the above simulations also show that there is a probability of a cluster at any redshift being selected for our survey, regardless of whether or not we can correctly determine the cluster’s redshift. Therefore, we need to determine over what range we can successfully measure the redshift of a cluster given our observational strategy. To estimate the probability of correctly determining a cluster’s redshift and, thus the range in redshifts we probed, we have combined the two different simulations discussed previously to construct mock redshift catalogs.

To simulate redshift distributions, we used the CFRS dataset from Section 4.1 to construct a background galaxy population. We used the above cluster models to predict the number of observable cluster members. We then model the redshift distribution of a cluster as a Gaussian with a standard deviation of  $500 \text{ km s}^{-1}$ . For every cluster candidate in our sample, we construct 10000 mock redshift distributions consisting of both cluster members and random galaxies from the CFRS catalog. Each redshift distribution has the number of redshifts set to match the total number of  $V_4 - I_4 > 1$  galaxy redshifts we successfully measured towards that cluster candidate. For example, for PDCS 62 we successfully measured six redshifts, however only five have a  $V_4 - I_4 > 1$ , thus our mock redshift catalogs would only have 5 redshifts. The magnitude limit of the mock redshift distribution is equal to faintest galaxy observed for that cluster candidate from Table 2.

By constructing mock redshift distributions and then applying our criteria for determining a cluster redshift from Section 4.1, we can determine the probability of detecting each cluster in our sample. We ran the simulations twice, once for the estimated

redshift from the original PDCS catalog and once using the “best” redshift from Table 3. For PDCS 57, which does not have a “best” redshift estimate, we only created these mock redshift catalogs for the estimated redshift. The results of these simulations showed that the failure rate became high for clusters with  $z > 0.4$ . For example, if PDCS 62 is a cluster at a redshift of 0.4665 (the redshift of the the closest pair), then we find that we would only have a 21.5% chance of detecting a triplet of galaxies all within  $1500 \text{ km s}^{-1}$  of the actual cluster redshift, despite the high richness of the system. These artificial redshift distributions show that we can successfully measure the redshift of Richness Class 1 and 2 clusters in our sample for  $z \leq 0.35$ , while for Richness Class 0 systems we must restrict our results to  $z \leq 0.3$ .

The above simulations of artificial redshift distributions have shown that we should be able to reliably calculate the surface and space density of PDCS clusters below a redshift of 0.3 regardless of the richness of these clusters. For Richness Class 1 and greater we can extend the range to 0.35. To ensure that the clusters are truly physical systems, we will restrict our analysis to those clusters with three or more concordant redshifts (as discussed above) and that are part of the complete sample of Holden *et al.* (1997). These restrictions leave the following clusters for our consideration: PDCS 02, 05, 34, 36, 38 and 40. Two of these clusters are Richness Class 0, three are Richness Class 1, and one is a Richness Class 2 cluster. If we restrict the redshift range to  $0.1 \leq z \leq 0.3$ , we have four PDCS clusters. Over the  $1.85 \text{ deg}^2$  (see Holden *et al.* 1997 for details on the area surveyed), these four clusters have a surface density of  $2.2_{-1.0}^{+1.7}$  clusters  $\text{deg}^{-2}$ . This surface density is in agreement with the bottom panel of Figure 21 of P96 for clusters with a  $\Lambda > 20$ , given our large error bars.

For the space density we need to compute the volume enclosed by the redshift range over the  $1.85 \text{ deg}^2$  surveyed by the sample . To compute this volume, we used the results plotted in Figure 4 and multiplied the probability of selection for each cluster by the volume element for each redshift interval (the simulations were performed at redshift intervals of  $\delta_z = 0.01$ ). In other words, instead of the usual Friedman-Robertson-Walker metric volume, we compute the volume as

$$V(z) = \Omega \int_{z_1}^{z_2} \frac{p(z)r^2 dr}{\sqrt{1 - kr^2}}$$

where  $p(z)$  represents the probability of a cluster being selected for our survey,  $\Omega = 1.85 \text{ deg}^2$ ,  $z_1 = 0.1$ ,  $z_2 = 0.35$  and  $k = 0$  for  $q_o = 0.5$ . We find that the computed space density of the three Richness Class 1 clusters (simply  $\frac{3}{V(z)}$ ) is  $31.3_{-17.1}^{+30.5} \times 10^{-6} h^3 \text{ Mpc}^{-3}$  ( $q_o = 0.5$ , 68% confidence limits for a Poisson distribution, see Gehrels 1986). For the same value of  $q_o$ , P96 measured  $20.2 \pm 8.1 \times 10^{-6} h^3 \text{ Mpc}^{-3}$  for Richness Classes 1 clusters. In the redshift range  $0.1 \leq z \leq 0.35$ , we also include PDCS 34, a Richness Class 2 cluster. This single Richness Class 2 cluster implies a space density for Richness Class 2 clusters of

$$10.4_{-8.4}^{+23.4} \times 10^{-6} h^3 \text{Mpc}^{-3}.$$

## 5. Discussion

Our survey had two goals, to test the accuracy of the matched-filter estimated redshift, and to estimate the surface and space density of PDCS clusters. We find that the matched-filter redshift estimate is at least as accurate as discussed in the original PDCS paper. Secondly, we find that the cumulative surface density and the space density of PDCS clusters at low redshifts agrees with the density found using the original catalog.

Our worst case estimate of the standard deviation for the matched-filter redshift measurements is 0.20 in  $z$ , the same error estimate quoted in the original paper of P96. However, if we restrict our sample to those eight clusters with three or more redshift in agreement, we find that the dispersion drops to 0.06 in redshift. This error is quite small and is comparable to the errors on photometric redshifts for individual galaxies (Brunner *et al.* 1997). Our measurement of the error in the matched-filter redshift most likely represents the best possible case for this algorithm. The majority of the clusters in our sample are at low redshifts compared to the majority of clusters in the PDCS ( $0.1 \leq z \leq 0.35$ ) and therefore the cluster members are the easy to separate from field galaxies. Also, as the cluster galaxies are at low redshift they are quite bright and thus, have the best measured magnitudes in the PDCS. For the higher redshift clusters in the PDCS, the error in the measured magnitudes of the cluster members should increase (as the magnitudes will be fainter) and there will be a higher surface density of field galaxies contaminating the cluster. Both of these effects will affect how well the matched-filter algorithm can estimate the redshift of the cluster. Nonetheless, the low apparent scatter in the estimated redshift for low redshift PDCS clusters shows the power of the matched-filter approach for characterizing cluster properties. With the addition of photometric redshifts, this technique should become even more accurate.

Our density measurements compare favorably with those found in the original PDCS catalog and are a factor of approximately  $7_{-4}^{+7}$  times higher than the Abell catalog cluster densities (see P96 and references therein for Abell cluster densities), though with large statistical errors. One of the questions raised by the original PDCS paper was why the PDCS has a space density of clusters of galaxies at low ( $z \leq 0.3$ ) redshifts  $\sim 5$  times greater than that of the Abell catalog. Though we have not answered this question, we have shown this is not because a large number of the PDCS cluster candidates are false positive detections. We independently estimated the space density of PDCS clusters using only the clusters with three or more measured redshifts within  $1500 \text{ km s}^{-1}$  of the median, a

criterion that occurs  $\sim 3\%$  of the time for triplets of field galaxies as seen in the CFRS. Therefore, our space density is based on likely physical systems.

To further explore the type of clusters detected by the PDCS, we have expanded our original survey to include more spectra per cluster as well as more clusters. This will allow us to measure velocity dispersions and therefore, the masses of the PDCS clusters, thus allowing us to directly compare with both the models of Press & Schechter (1974), Bahcall *et al.* (1997) and Reichart *et al.* (1999) and with the Abell catalog using such samples as the ESO Nearby Abell Cluster Sample (Katgert *et al.* 1996) or the catalog of Girardi *et al.* (1998). By making comparisons with other samples, we will be able to understand the discrepancy between the space density of the PDCS clusters and those found in the Abell catalog. By comparing with the models, we will then continue the process of using such a catalog to constrain models of cluster formation and evolution. Nonetheless, the agreement between our measured space densities and the densities quoted by the original PDCS is an important verification of the PDCS cluster catalog.

## 6. Summary

The goal of our spectroscopic survey was to test the main results of the original Palomar Distant Cluster Survey (PDCS) paper (P96). We achieved this goal by observing a subsample of PDCS clusters for multi-object spectroscopy that was chosen as independently as possible from the parameters of the original PDCS catalog. We selected our sample from those PDCS cluster candidates with the largest number of  $V_4 < 21$ ,  $V_4 - I_4 > 1$  galaxies in the spectrograph field of view. We chose these criteria to select likely cluster members that were observable with the instrumentation available. We obtained 130 spectra of galaxies in the direction of sixteen PDCS cluster candidates. Due to bad weather, only 84 of these 130 spectra yielded a secure redshift measurement.

We successfully obtained at least three redshift measurements for every PDCS cluster candidate in our sample. Using Monte Carlo simulations of the Canada-France Redshift Survey, we have shown that a secure cluster redshift can be obtained from such a small amount of data, if one restricts the analysis to clusters with three or more concordant redshifts within  $1500 \text{ km s}^{-1}$  of the median redshift. This only occurred  $\sim 3\%$  of the time within our Monte Carlo simulations of the Canada-France Redshift Survey. Eight of the sixteen PDCS clusters observed satisfy this requirement and lie in the redshift range  $0.1 \leq z \leq 0.35$ .

If we restrict ourselves to this subsample of eight clusters, the observed standard

deviation between the spectroscopically measured redshift for the clusters and the matched-filter estimated redshifts (given by P96) is  $\sigma_z = 0.06$ . If we consider all fifteen PDCS clusters in our sample with at least two galaxies at the same redshift, this observed standard deviation rises to  $\delta_z = 0.20$ , a value consistent with the error quoted by P96.

Using detailed simulations of our target selection procedure, we have measured the space densities of Richness Class 1 and 2 PDCS clusters. We are in close agreement with the space densities quoted in P96 *i.e.* that the observed space density of  $0.1 \leq z \leq 0.3$  PDCS clusters is a factor of  $\sim 5$  greater than that observed nearby from the Abell Catalog. However, we note that our measurements are  $\sim 7_{-4}^{+7}$  greater than the Abell Catalog space density. We hope to build this on sample in order to investigate those properties of PDCS clusters important for cosmological studies *e.g.* redshift distribution, richness function, and mass function. With this information, will be able to answer the important question of what sort of clusters the PDCS is finding.

## 7. Acknowledgments

We would like to thank Richard Kron for useful discussions on sample selection, Francisco Castander and Marianne Takamiya for help with the spectroscopic data reduction, and Constance Rockosi for helpful comments on an early draft of this paper. Finally, we would like to thank Jim DeVeney of NOAO for his help in the mask preparation and instrument setup. This project was funded in part by NASA grant NAG5-3202. BH was partially supported by the Center for Astrophysical Research in Antarctica, a National Science Foundation Science and Technology Center.

## REFERENCES

- Abell, G.O., 1958, ApJS, 3, 211
- Abell, G.O., Corwin, H.G. Jr., Olowin, R.P., 1989, ApJS, 70, 1
- Bahcall, N.A., Fan, X., & Cen, R. 1997, ApJ, 485, 53
- Brunner, R.J., Connolly, A.J., Szalay, A.S., & Bershadsky, M.A. 1997, ApJ, 482, 21
- Burke, D. J., Collins, C. A., Sharples, R. M., Romer, A. K., Holden, B. P. & Nichol, R. C. 1997, ApJ, 488, L83

- Carlberg, R. G., Yee, H. K. E., Ellingston, E., Abraham, R., Gravel, P., Morris, S. & Pritchett, C. J. 1996, *ApJ*, 462, 32
- Coleman, G.D., Wu, C.C. & Weedman, D.W. 1980, *ApJS*, 43, 393
- Colless, M. 1989, *MNRAS*, 237, 799
- Couch, W.J., Ellis, R.S., MacLaren, I. & Malin, D.F. 1991, *MNRAS*, 249, 606
- Crampton, D., Le Fevre, O., Lilly, S. J., & Hammer, F. 1995, *ApJ*, 455, 96
- Dalton, G. B., Efstathiou, G., Maddox, S. J., & Sutherland, W. J. 1992, *ApJ*, 380, L1
- Ebeling, H., Edge, A. C., Fabian, A. C., Allen, S. W., Crawford, C. S. & Bohringer, H. 1997, *ApJ*, 479, L101
- Ellingston, E. 1989, *A User's Guide to Multislit Reductions with IRAF (NOAO Manual)*
- Girardi, M., Giuliano, G., Mardirossian, F., Mezzetti, M., & Boschin, W. 1998, *ApJ*, 505, 74
- Gehrels, F. 1986, *ApJ*, 303, 336
- Gunn, J.E., Hoessel, J.G., & Oke, J.B. 1986, *ApJ*, 306, 30
- Hammer, F., Crampton, D., Le Fevre, O., & Lilly, S. J. 1995, *ApJ*, 455, 88
- Henry, J.P., Gioia, L., Maccacaro, T., Morris, S.L., Stocke, J., & Wolter, A. 1992, *ApJ*, 386, 408
- Holden, B. P., Romer, A. K., Nichol, R. C., & Ulmer, M. P. 1997, *AJ*, 114, 1701
- Isobe, T., Feigelson, E.D., & Nelson, P.I. 1986, *ApJ*, 306, 490
- Katgert, P., Mazure, A., Perea, J., Den Hartog, R., Moles, M., Le Fevre, O., Dubath, P., Focardi, P., Rhee, G., Jones, B., Escalera, E., Biviano, A., Gerbal, D., & Giuricin, G. 1996, *A&A*, 310, 8
- Kurtz, M, & Mink, D. 1998, *PASP*, 110, 934
- Lacey, C. & Cole, S. 1993, *MNRAS*, 262, 627
- Lidman, C. E. & Peterson, B.A. 1996, *AJ*, 112, 2454
- Lilly, S. J., Le Fevre, O., Crampton, D., Hammer, F., & Tresse, L. 1995, *ApJ*, 455, 50

- Le Fevre, O., Crampton, D., Lilly, S. J., Hammer, F., & Tresse, L. 1995, *ApJ*, 455, 60
- Lubin, L.M., & Postman, M.P. 1996, *AJ*, 111, 1795
- Lubin, L.M. 1996, *AJ*, 112, 23
- Lumsden, S. L., Nichol, R. C., Collins, C. A., & Guzzo, L. 1992, *MNRAS*, 258, 1
- Nichol, R. C., Holden, B. P., Romer, A. K., Ulmer, M. P., Burke, D. J. & Collins, C. A. 1997, *ApJ*, 481, 644
- Olsen, L.F. *et al.* 1999a, *A&A*, 345, 363
- Olsen, L.F. *et al.* 1999b, *A&A*, 345, 681
- Ostrander, E. J., Nichol, R. C., Ratnatunga, K. U., Griffiths, R. E. 1998, *AJ*, 116, 2644
- Oukbir, J. & Blanchard, A. 1997, *A&A*, 317, 1
- Press, W. H., & Schechter, P. 1974, *ApJ*, 187, 425
- Postman, M.P., Lubin, L.M., Gunn, J.E., Oke, J.B., Hoessel, J.G., Schneider, D.P., & Christensen, J.A. 1996, *AJ*, 111, 615 (P96)
- Postman, M.P., Lauer, T.R., Szapudi, I., & Oegerle, W. 1998, *ApJ*, 506, 33
- Reichart, D. E., Nichol, R. C., Castander, F. J., Burke, D. J., Collins, C. A., Romer, A. K., & Holden, B. P. 1999, *ApJ*, accepted
- Tonry, J., & Davis, M. 1979, *AJ*, 84, 1511
- Viana, P. P. & Liddle, A. R. 1996, *MNRAS*, 281, 323
- Zaritsky, D., Nelson, A.E., Dalcanton, J.J., Gonzalez, A.H. 1997, *ApJ*, 480, 91

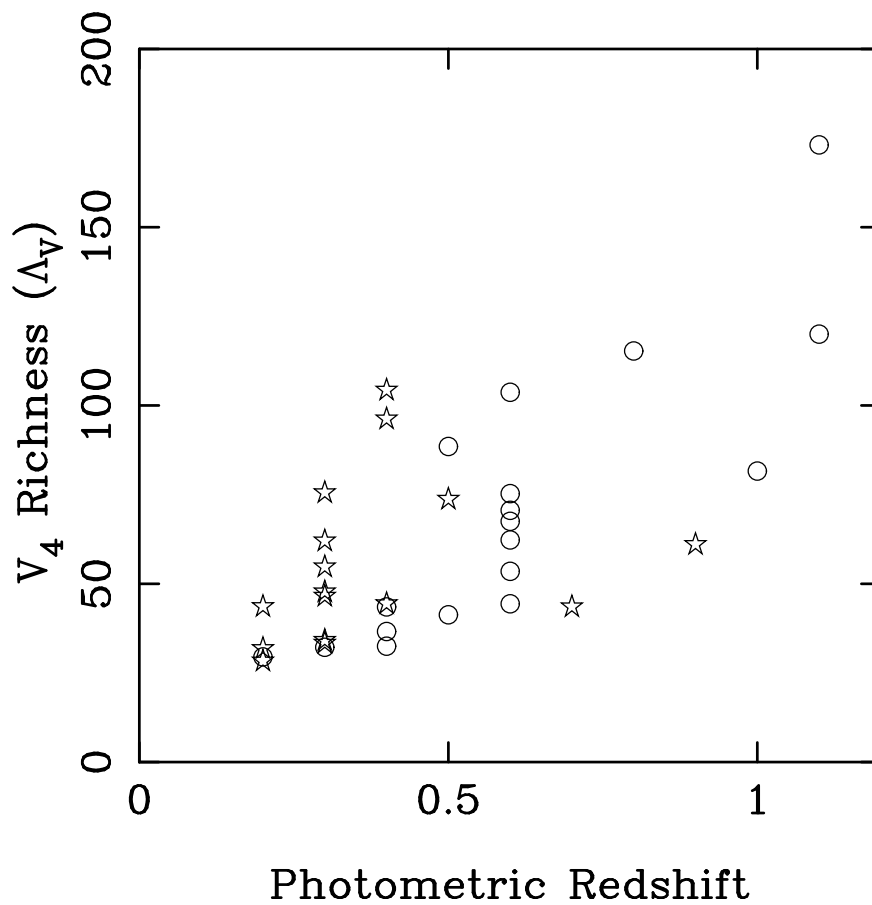


Fig. 1.— The estimated matched-filter redshift versus the observed  $V_4$  richness for PDCS cluster candidates. The stars symbols represent the sixteen clusters observed and discussed herein while the circle symbols are other PDCS in our sample that were not observed.

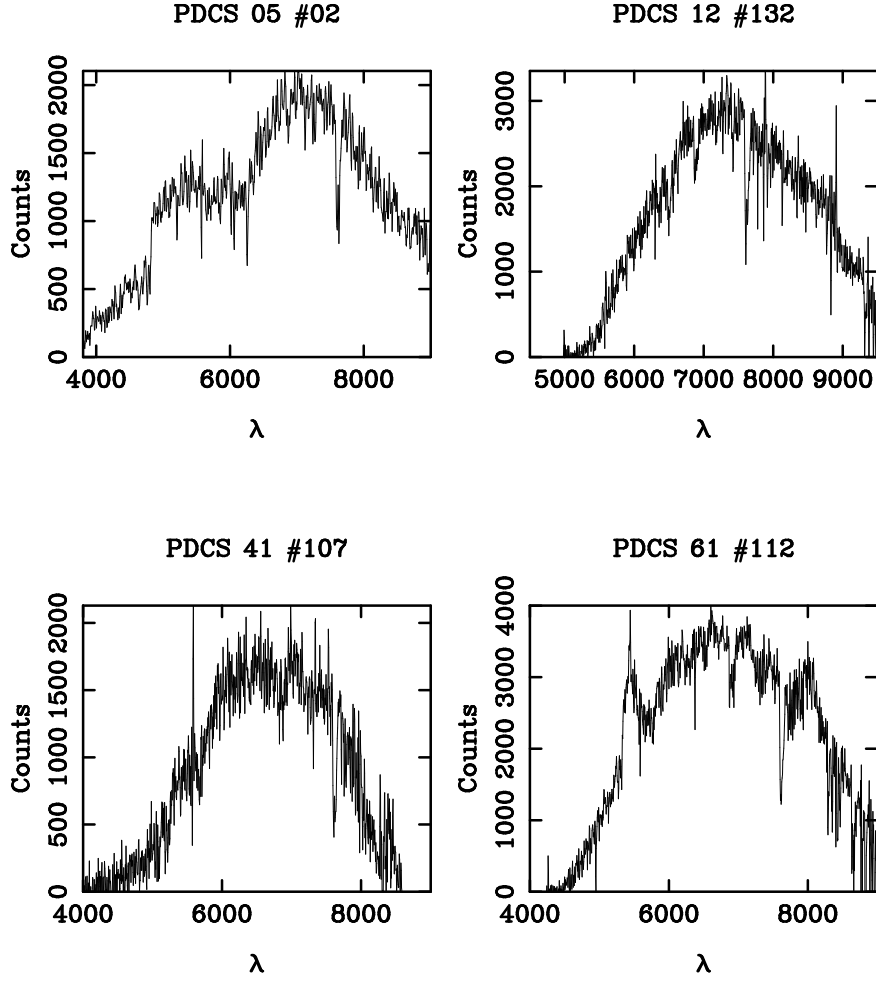


Fig. 2.— We plot representative spectra. The upper left-hand plot is PDCS 05 # 2 ( $z=0.2112$ ,  $r=6.05$ ) which was observed with the ARC 3.5m Double Imaging Spectrograph. The spectrum shows both the blue and red camera data. The upper right-hand plot is PDCS 12 # 132 ( $z=0.2585$ ,  $r=4.67$ ), a spectrum from CryoCam using the 780-2 Grism. In the lower left-hand corner, we plot PDCS 41 # 107 ( $z=0.3171$ ,  $r=4.51$ ), observed on CryoCam with the 770 Grism. The spectrum in the lower right-hand corner is a potential active galactic nucleus found in our sample (PDCS 61 # 112) which has a tentative redshift of 0.94 based on the one emission feature at 5437  $\text{\AA}$ .



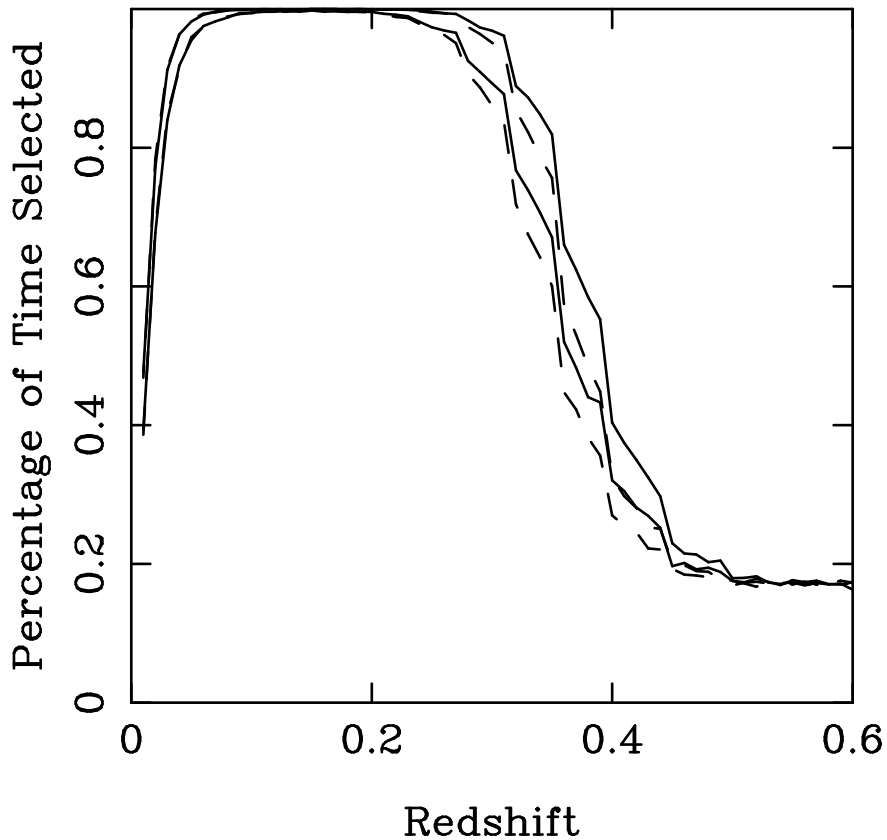


Fig. 4.— Here we show the probability of selecting a PDCS cluster for observation as a function of redshift for  $q_o = 0.5$  (solid lines) and  $q_o = 0.1$  (dashed lines). The upper pair of lines represents the probability of detecting a Richness Class 2 cluster, while the bottom pair of lines is for Richness Class 1 cluster.

TABLE 1. PDCS Cluster Observed

PDCS # <sup>a</sup>	$\alpha^b$ (J2000.0)	$\delta^b$ (J2000.0)	Exp Time <sup>c</sup> s	Number of <sup>d</sup> Galaxies Observed	Net Number <sup>e</sup> of Galaxies	Observatory
02	00 29 28.4	+05 04 03	1200 & 2700	4	12.0	APO & KPNO2
05	00 27 38.6	+05 09 46	1200	4	5.0	APO
11	00:29:44.9	+05:51:44	5400	10		KPNO2
12	00 27 59.8	+05 56 28	3600	12		KPNO2
23	02 27 56.1	+01 05 15	5753	8		KPNO2
30	09 54 46.3	+47 10 48	8100	9	5.7	KPNO1
34	09 55 06.1	+47 29 56	3600	8	3.7	KPNO1
36	09 53 53.7	+47 40 16	7200	10	9.7	KPNO1
38	09 51 09.9	+47 43 55	3600	7	4.7	KPNO1
40	09 53 26.0	+47 58 57	3600	9	7.7	KPNO1
41	09 54 24.9	+47 58 49	5400	7	2.7	KPNO1
42	09 53 48.4	+47 57 57	3600	6	3.7	KPNO1
57	13 23 47.9	+30 03 24	5400	8	2.5	KPNO1
60	13 23 42.7	+30 10 08	3600	4	4.5	KPNO1
61	13 27 02.4	+30 18 14	5400	7	2.5	KPNO1
62	13 23 42.2	+30 22 38	5400	7	4.5	KPNO1

<sup>a</sup>The PDCS identification number.

<sup>b</sup>The mask center positions, not the PDCS centroids.

<sup>c</sup>The total exposure time for the galaxies observed.

<sup>d</sup>The number of slitlets cut for a mask or the number galaxies observed with a long slit.

<sup>e</sup>The net number of galaxies observed within 2'5 of the PDCS cluster centroid that met our color and magnitude criteria. PDCS 11, 12 & 23 are not part of our complete sample so our missing this number. See text for details.

TABLE 2. Galaxy Observations

PDCS <sup>a</sup> ID #	<i>Galaxy</i> ID #	$\alpha^b$ (J2000.0)	$\delta^b$ (J2000.0)	$V^c$	$V - I^c$	$z$	$\sigma_z^d$	$r^e$
02	01	00:29:23.15	+05:04:27.6	18.74	1.24	0.2093	0.0003	5.44
02	02	00:29:36.36	+05:03:16.8	18.98	1.29	0.2067	0.0003	3.44
02	03	00:29:36.89	+05:03:05.7	19.42	1.43	0.2447	0.0003	3.94
02	04	00:29:36.23	+05:04:53.8	19.59	1.59	0.2841	0.0001	5.97
02	105	00:29:23.42	+05:02:40.8	20.36	1.27	0.2463	0.0004	3.72
02	111	00:29:26.93	+05:03:43.1	19.80	1.39	0.2474	0.0003	4.03
02	119	00:29:36.23	+05:04:53.8	19.59	1.59	0.2850	0.0003	5.15
05	01	00:27:36.83	+05:09:41.8	17.79	1.26	0.2131	0.0002	6.09
05	02	00:27:37.06	+05:09:31.5	18.35	1.09	0.2112	0.0002	6.05
05	03	00:27:43.90	+05:09:24.4	18.70	1.10	0.2082	0.0003	3.06
11	112	00:29:36.73	+05:51:40.6	20.22	1.79	0.4194	0.0004	3.90
11	106	00:29:42.26	+05:51:04.0	20.37	1.68	0.3266	0.0004	4.32
11	105	00:29:47.23	+05:50:47.6	19.81	1.82	0.3204	0.0002	6.25
12	111	00:27:50.81	+05:55:36.0	20.22	1.28	0.2644	0.0004	3.21
12	109	00:27:52.22	+05:55:31.3	19.67	1.42	0.2635	0.0003	5.95
12	105	00:27:55.92	+05:55:10.3	19.89	1.06	0.2611	0.0003	3.70
12	124	00:27:55.29	+05:57:00.3	20.94	1.27	0.2633	0.0004	3.07
12	122	00:27:56.84	+05:56:40.4	20.94	1.37	0.2634	0.0003	3.34
12	130	00:27:56.25	+05:58:00.0	20.65	1.35	0.3104	0.0004	3.86
12	131	00:27:57.34	+05:58:00.4	20.43	1.57	0.3103	0.0004	3.31
12	116	00:28:00.38	+05:56:23.6	19.27	1.24	0.2595	0.0002	6.32
12	132	00:28:06.32	+05:58:05.9	19.65	1.35	0.2585	0.0003	4.66
23	117	02:27:46.41	+01:05:13.1	19.75	1.61	0.1302	0.0002	5.92
23	118	02:27:48.87	+01:05:16.4	16.85	1.15	0.1298	0.0002	7.34
23	125	02:27:53.36	+01:05:58.8	20.97	1.39	0.3020	0.0004	3.07
23	112	02:27:54.00	+01:04:47.5	18.97	1.11	0.1275	0.0002	5.05
23	123	02:27:58.68	+01:05:53.9	17.49	1.39	0.1285	0.0003	3.62
23	108	02:28:00.15	+01:04:34.0	17.71	0.84	0.1288	0.0003	3.19
23	102	02:27:59.81	+01:03:18.8	17.96	1.34	0.1280	0.0004	3.03
30	103	09:54:39.58	+47:08:44.9	19.88	1.36	0.2513	0.0003	4.06
30	102	09:54:44.03	+47:08:36.5	20.10	1.53	0.4578	0.0003	3.87
30	107	09:54:38.38	+47:10:24.8	19.20	1.08	0.2506	0.0002	6.10
30	104	09:54:46.32	+47:09:50.2	19.63	0.99	0.2889	0.0003	e-4
34	103	09:55:03.47	+47:28:33.5	19.73	1.32	0.3288	0.0003	3.70
34	104	09:55:06.07	+47:29:04.3	19.67	1.58	0.3338	0.0002	7.57
34	105	09:55:04.26	+47:29:49.4	20.98	0.64	0.3853	0.0006	3.36
34	107	09:55:09.00	+47:29:52.9	19.75	1.64	0.3322	0.0002	7.09
34	111	09:55:12.78	+47:30:31.4	20.99	1.56	0.3354	0.0004	3.26
34	113	09:55:19.81	+47:30:47.5	20.78	0.88	0.0776	0.0003	4.16
36	107	09:53:48.07	+47:39:05.4	20.84	1.55	0.2775	0.0004	3.12
36	111	09:53:49.25	+47:39:43.8	19.57	1.41	0.3310	0.0002	7.51
36	109	09:53:57.18	+47:39:14.6	19.72	1.29	0.2507	0.0002	7.49
36	114	09:53:54.16	+47:40:22.1	18.59	1.43	0.2495	0.0002	11.51
36	112	09:54:03.91	+47:40:03.9	20.47	1.31	0.2473	0.0003	3.84
36	118	09:54:05.30	+47:41:32.4	19.84	1.25	0.2503	0.0002	9.23
38	112	09:51:11.13	+47:46:16.4	20.53	1.17	0.3340	0.0003	3.65
38	109	09:51:07.04	+47:44:06.9	20.09	1.54	0.3339	0.0002	7.47
38	110	09:51:10.41	+47:44:09.3	19.80	1.53	0.3345	0.0002	9.37

TABLE 2. (continued)

PDCS <sup>a</sup> ID #	<i>Galaxy</i> ID #	$\alpha^b$ (J2000.0)	$\delta^b$ (J2000.0)	$V^c$	$V - I^c$	$z$	$\sigma_z^d$	$r^e$
38	107	09:51:08.91	+47:43:43.2	20.47	1.66	0.3354	0.0003	5.83
40	117	09:53:14.52	+47:59:59.8	19.39	1.17	0.2024	0.0002	7.14
40	116	09:53:28.54	+47:59:43.9	19.26	1.40	0.2046	0.0002	7.00
40	109	09:53:38.38	+47:58:30.0	19.69	1.12	0.2028	0.0002	10.54
40	105	09:53:23.85	+47:57:38.0	18.58	1.27	0.2013	0.0003	3.39
40	104	09:53:20.68	+47:57:00.2	20.30	1.14	0.2052	0.0004	3.11
41	108	09:54:24.53	+47:58:57.8	20.53	1.28	0.2971	0.0003	3.85
41	106	09:54:27.05	+47:58:52.3	19.64	1.40	0.2963	0.0004	3.12
41	107	09:54:28.71	+47:58:55.9	20.27	1.55	0.3171	0.0003	4.51
41	109	09:54:30.65	+48:00:19.6	20.13	1.82	0.3728	0.0003	4.82
42	104	09:53:51.95	+47:55:54.5	20.78	1.56	0.0869	0.0008	3.27
42	109	09:53:38.38	+47:58:30.0	19.69	1.12	0.1982	0.0002	5.76
42	107	09:53:49.04	+47:58:26.9	20.60	1.35	0.5355	0.0003	e-4
42	105	09:54:00.92	+47:58:03.6	20.83	1.76	0.5369	0.0003	3.27
42	111	09:53:45.93	+47:59:08.8	19.69	1.22	0.2001	0.0002	7.86
57	111	13:23:42.24	+30:04:47.4	20.44	1.35	0.2546	0.0003	5.05
57	110	13:23:44.84	+30:04:12.7	17.56	1.05	0.1604	0.0003	4.63
57	110	13:23:44.84	+30:04:12.7	17.56	1.05	0.1596		e-1
57	107	13:23:43.96	+30:03:31.5	20.83	1.64	0.0693	0.0003	3.45
57	106	13:23:48.24	+30:03:29.6	19.55	1.54	0.3033	0.0003	4.87
57	105	13:23:48.35	+30:03:04.8	19.90	0.45	0.4808	0.0003	3.04
57	108	13:23:55.55	+30:03:53.7	20.52	0.91	0.4073	0.0003	3.34
60	102	13:23:38.67	+30:10:00.8	19.41	1.16	0.3258	0.0004	3.78
60	106	13:23:37.12	+30:11:52.3	19.24	1.14	0.2004	0.0002	6.34
60	105	13:23:39.12	+30:11:52.0	19.88	1.14	0.1990	0.0003	4.28
61	111	13:26:53.10	+30:18:17.6	20.37	1.65	0.3453	0.0003	5.55
61	112	13:26:57.97	+30:20:23.3	19.96	1.80	0.94		e-1
61	102	13:26:58.68	+30:16:12.9	20.97	1.16	0.4314	0.0004	3.23
61	103	13:27:00.94	+30:16:37.8	19.54	0.20	0.1255	0.0005	e-6
61	108	13:27:05.27	+30:18:03.3	19.78	1.15	0.1710	0.0004	3.76
61	107	13:27:06.75	+30:17:54.2	19.42	1.52	0.1716	0.0002	6.71
62	103	13:23:34.09	+30:21:16.3	20.01	1.39	0.2945	0.0005	3.77
62	105	13:23:41.83	+30:21:52.8	19.26	0.03	0.0610	0.0005	e-4
62	107	13:23:39.69	+30:22:20.4	20.87	2.05	0.4638	0.0003	3.88
62	110	13:23:37.16	+30:22:52.8	20.90	1.66	0.4536	0.0003	3.08
62	113	13:23:35.37	+30:23:22.4	19.77	1.16	0.0822	0.0002	3.17
62	114	13:23:36.18	+30:23:50.9	20.91	2.15	0.4685	0.0004	3.38

<sup>a</sup>The PDCS cluster identification number. PDCS 57 # 2 is mentioned twice as its redshift was determined by absorption lines and an emission line.

<sup>b</sup>The galaxy position in J2000 coordinates as derived in the original PDCS catalog, see Postman *et al.* 1996 for details.

<sup>c</sup>The galaxy magnitude and color in the 4-shooter filter system as described in the PDCS.

<sup>d</sup>Error in cross-correlation for absorption spectra or error in fit to emission features.

<sup>e</sup> $r$  value from Tonry & Davis for cross-correlation Spectra with the letter e have emission lines, the number of lines follows the letter e.

TABLE 3. Cluster Redshifts

PDCS # <sup>a</sup>	$z_{\text{matched-filter}}$	$z_{\text{median}}$ <sup>b</sup>	$z_{\text{best}}$ <sup>c</sup>	$\text{err}_z$ <sup>d</sup>	Fraction used <sup>e</sup>	Richness Class <sup>f</sup>
02	0.4	0.2463	0.2463	11089	3/7	1/1
05	0.2	0.2112	0.2112	579	3/3	0/0
11	0.4	0.3266	0.3235		2/3	3/1
12	0.3	0.2634	0.2634	699	6/8	2/2
23	0.2	0.1288	0.1288	300	6/7	1/1
30	0.3	0.2509	0.2594		2/4	1/0
34	0.3	0.3330	0.3330	986	4/6	2/2
36	0.3	0.2505	0.2505	628	5/6	1/1
38	0.3	0.3342	0.3342	84	4/4	1/0
40	0.2	0.2028	0.2028	444	5/5	0/0
41	0.7	0.3071	0.2997		2/4	1/1
42	0.9	0.1992	0.1992		2/5	2/2
57	0.5	0.2790				2/2
60	0.3	0.2004	0.1997		2/3	0/0
61	0.3	0.2585	0.1712		2/5	0/1
62	0.4	0.3740	0.4665		2/6	3/3

<sup>a</sup>The PDCS identification number.

<sup>b</sup>The median of all the galaxy redshifts from Table 2.

<sup>c</sup>The “best” estimated redshift. This is either the median redshift if three or more galaxies are within  $1500 \text{ km s}^{-1}$  of the median or is the average redshift of a pair galaxies within  $1500 \text{ km s}^{-1}$ , see text for details.

<sup>d</sup>The error on the estimated redshift in kilometers per second. For clusters where only two galaxies were used to determine the “best” estimated redshift, no error was calculated.

<sup>e</sup>The fraction of all galaxies with redshifts used to determine the “best” estimated redshift, see text for details.

<sup>f</sup>The Richness Class as estimated in both the  $V_4$  and  $I_4$  bands. See Sec 4.3 for definitions of Richness Classes in terms of  $\Lambda_{cl}$